Investigating the adaptability of the multi-pump multi-piston power take-off system for a novel wave energy converter

Wei, Y.; Barradas Berglind, J.J; van Rooij, M.; Prins, WA; Jayawardhana, B.; Vakis, A. I.

Published in:
Renewable Energy

DOI:
10.1016/j.renene.2017.04.042

Publication date:
2017

Investigating the Adaptability of the Multi-Pump Multi-Piston Power Take-Off System for a Novel Wave Energy Converter

Y. Wei[a], J. J. Barradas Berglind[b], M. van Rooij[a], W. A. Prins[a], B. Jayawardhana[b], A. I. Vakis[a,*]

[a] *Advanced Production Engineering, Engineering and Technology Institute Groningen, Faculty of Science & Engineering, University of Groningen, Nijenborgh 4, Groningen 9747AG, The Netherlands*

[b] *Discrete Technology & Production Automation, Engineering and Technology Institute Groningen, Faculty of Science & Engineering, University of Groningen, Nijenborgh 4, Groningen 9747AG, The Netherlands*

Abstract

In this work, a numerical model is developed in order to investigate the adaptability of the multi-pump multi-piston power take-off (MP^2PTO) system of a novel wave energy converter (WEC). This model is realized in the MATLAB/SIMULINK environment, using the multi-body dynamics solver Multibody^{TM}, which is based on the open-source tool WEC-Sim. Furthermore, the hydrodynamic coefficients are calculated using the open-source code NEMOH. After providing the description of the model, it is validated against experimental results and an analytical model, showing good agreement with both. Subsequently, simulations for a single floater device with a multi-piston pump (MPP) unit using our numerical model are carried out to demonstrate the adaptability of the WEC. In addition, the results demonstrate that the MPP with a simple control strategy can extract more energy than any non-adaptable piston pump under various sea states. Finally, a floater blanket (an array of interconnected floaters) model is developed to shed some light on the hydrodynamic response and the performance of MPPs. The developed numerical model will be used in the future to optimize the MP^2PTO configuration, and to develop an energy maximization control strategy for the MP^2PTO system.

Keywords: Ocean Grazer, wave and multi-body interaction, floater blanket, MP^2PTO system

1. Introduction

Wave energy converters (WECs) are devices designed to transform the motion of ocean waves into electricity. Although hundreds of WECs have been conceptualized and patented for over a century (McCormick, 1981), wave energy technologies have not yet converged to

*Corresponding author
Email address: a.vakis@rug.nl (A. I. Vakis)

a universal standard conceptual design as is the case, for instance, with three-bladed wind turbines for wind energy harvesting. Various new concepts of WECs have been proposed, and a number of small prototypes have been tested during the last decades based on point absorbers, attenuators and other designs (Li and Yu, 2012). The recently proposed novel WEC constituting the core technology of the Ocean Grazer (Prins, 2013) has the potential to be an effective contender in the challenge to extract the energy from offshore ocean waves, across the sea states relevant to energetic deployment locations such as the coasts of Ireland and Scotland.

A single Ocean Grazer device is projected to be a massive platform housing various renewable energy generation modules, including wave, wind and solar, obtaining the majority of its energy input from ocean waves. The core innovation of its WEC, namely the *multi-pump multi-piston power take-off* (MP^2PTO) system, consists of a grid of interconnected floater elements (which we term as a *floater blanket*), with each floater being connected to a piston-type hydraulic pumping system, a *multi-piston pump* (MPP) (Prins, 2013; Vakis and Anagnostopoulos, 2016). Each pumping system consists of three differently-sized engageable pistons, allowing for seven different pumping combinations; this working principle gives the system its adaptability, thus allowing it to efficiently extract energy from incident waves with varying periods and heights.

To validate the Ocean Grazer WEC concept, a 1:35 scale proof-of-concept-prototype with ten interconnected floater members has been developed at the University of Groningen. This experimental setup has enabled the successful testing of the functionality and the energy harvesting capabilities of the device. Preliminary results also confirmed the adaptability of the system to maximize energy extraction under various wave conditions. In order to investigate the hydraulics of the pumping system, a benchmark experiment of dynamical contact models of a single-piston pump (SPP) was carried out by van Rooij et al. (2015). A mathematical SPP model was also proposed to predict the piston dynamics and the efficiency of an SPP, and the comparison showed that the model had sufficient accuracy to describe the behaviour of the SPP. Vakis and Anagnostopoulos (2016) developed an analytical model for the SPP, which took into account the hydrodynamics of the floater and the elastohydrodynamic lubrication of the piston-cylinder interface. Their results pointed out that the mechanical efficiency of the system was close to 99%, while the pumping efficiency was dominated by volumetric losses. Note that the hydrodynamics models used in these studies were simplified by partly omitting the hydrodynamic effects of radiation and diffraction and could not account for hydrodynamic and mechanical interaction between the floater elements, since they only investigated a single floater system. For studying the adaptability and efficiency of our MP^2PTO system in particular, with the use of the floater blanket and multi-piston pump units, we extend the aforementioned SPP model in this paper in several directions. Firstly, we incorporate the hydrodynamics effects of radiation and diffraction. Secondly, we take into account mechanical joint coupling between the floaters. Lastly, we integrate the model multi-piston system into the comprehensive model. The development of a comprehensive hydrodynamic model of the floater blanket within the MP^2PTO system is desired to further prove the adaptability concept and perform an energy capture optimization study for the MP^2PTO system.

Subsequently, the development of advanced control systems is crucial in enabling the adapt-

ability and optimal operation of WECs to the energy content. A comprehensive overview of the general research literature relating to the control of WECs and wave-energy arrays (farms) can be found in Ringwood et al. (2014). For the optimal operation of our Ocean Grazer device, there are a number of critical sub-systems that require advanced control systems. For example, taking advantage of the adaptability of the MP^{2}PTO, Barradas-Berglind et al. (2016) developed a preliminary model predictive control (MPC) strategy aimed at maximizing the energy extraction of the SPP model from Vakis and Anagnostopoulos (2016) and made a preliminary analysis on the energy capture of a floater blanket consisting of five independent floater elements. The results showed that the energy capture could be optimized with a suitable MPC algorithm. Dijkstra et al. (2016) proposed a nonlinear optimization-based control strategy that maximizes the revenue of the Ocean Grazer device by exploiting its storage capabilities. The results indicated that the proposed strategy could effectively maximize the total revenue. Although positive results have been demonstrated by these preliminary investigations, it is still a great challenge to develop distributed control strategies for an Ocean Grazer device that consists of hundreds of interconnected floater elements. Control in wave energy applications may rely strongly upon an accurate and efficient hydrodynamic model, but taking into account the interconnections and multibody-wave interactions would increase the complexity and computational cost of the model. Development of computationally affordable hydrodynamic models, which can be used as bases for model-based control design, is worthy of investigation.

There are several WEC concepts similar to the floater blanket of the Ocean Grazer, which consists of an array of hydrodynamic elements. For example, the Hagen-Cockereil WEC (Haren and Mei, 1982) and the Pelamis WEC (Rainey, 2001) are both trains of slender rafts with power converters attached at the connecting hinges to extract energy from the relative rotation of neighbouring rafts. Another related concept, called CWEC (Alam, 2012), is a viscoelastic carpet placed over a network of vertically oriented springs and generators on the coastal seafloor. In these devices, each hydrodynamic element is not only excited by the incident waves, but also influenced by superposition of the diffracted and radiated waves from other elements; hence, hydrodynamic investigations on the devices essentially solve the wave and multi-body interaction problem. The hydrodynamic coefficients were obtained numerically or mathematically, and then, based on a linear PTO force assumption, the problems were solved by dealing with the motion equations in the frequency domain. In our case, however, due to the discontinuous nonlinearity in our MP^{2}PTO system (the pumping force can be very large during the upstroke, but becomes zero during the downstroke), the linearization of the present PTO force may require further experimental validation. At the current stage, with the aim to develop a proof-of-concept numerical model, it is decided to develop the model in the time domain, which makes it directly comparable with the experimental data. Furthermore, a time domain model may be applied to develop the control strategy for the MP^{2}PTO system.

To deliver a preliminary proof-of-concept model for the core technology of the Ocean Grazer, the research focus of this paper is twofold: (1) to validate the adaptability of an MPP with a single floater; and, (2) to understand the hydrodynamic response of the floater blanket and the energy extraction characteristics of the MP^{2}PTO system. The remainder of the paper is organized as follows: the numerical model is described in Section 2. Consequently, the model is validated in Section 3.1 by comparing it against experimental results and the previously

developed numerical model. The capture factor matrix of the MP^{2}PTO is presented in Section 3.2, followed by a set of simulations of the model under a random wave, i.e., using waves with varying periods and heights, to demonstrate the adaptability of the MPP concept. The hydrodynamics of the floater blanket and the performance of the MP^{2}PTO system are discussed in Section 3.3. Lastly, conclusions and further research points are given in Section 4.

2. Numerical model description

A schematic representation of the MP^{2}PTO system is shown in Fig. 1 for a floater blanket with four floater elements. The floater elements B1-B4 are physically interconnected, thereby assembled into the "blanket", which is excited under incident waves. The heaving motion of each floater element is transformed into the translational motion of pistons in an MPP unit, shown as P1-P4, by means of a rod. In this system, there are constraints at the top of the upper reservoir restricting the rod in the cylinder to move in the vertical direction, while allowing the upper part to have a relative rotation. Each MPP consists of three variable-size pistons resulting in seven different piston activation combinations, which allow a variable PTO load to be tuned to the incident waves, as shown in Fig. 1b. Thus, the MPP will extract energy while the interconnected floater radiates the incident waves, which in turn influence the dynamics of other floaters. Taking into account the complex wave field of the multi-floater interaction and the mechanics of the interconnection, multiple pistons can be activated within each pump independently. The series of floaters B1-B4 and MPP units P1-P4 compose the MP^{2}PTO system; when this MP^{2}PTO system is operated by a high-efficiency control system, it is expected that it will maximize the energy capture from ocean waves.

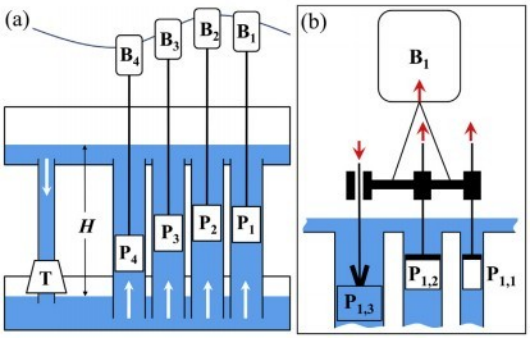

Figure 1: The Ocean Grazer WEC (Vakis and Anagnostopoulos, 2016): (a) the MP^{2}PTO system; (b) the multi-piston pump concept.

The dynamic response of the floater blanket with the MP^{2}PTO system can be described by a set of motion equations for multi-body systems. We consider that, as the incident waves interact with the floater blanket, each floater element moves along three degrees of freedom with one rotational (pitch) and two translational (surge and heave) displacements. The corresponding displacements and forces on each floater element can be obtained by solving the well-known Cummins' equation expressed below:

$$(\boldsymbol{M}_f + \boldsymbol{M}_\infty)\,\ddot{\boldsymbol{X}}_f + \int_0^t \boldsymbol{K}_r(t-\tau)\dot{\boldsymbol{X}}(\tau)\,d\tau = \boldsymbol{F}_{ext} + \boldsymbol{F}_B + \boldsymbol{F}_\nu + \boldsymbol{F}_{ic} + \boldsymbol{F}_{fr}, \qquad (1)$$

where $\boldsymbol{M}_f$ are the components of the generalized mass matrix of the floaters; $\boldsymbol{M}_\infty$ is the infinite-frequency added mass matrix; and $\boldsymbol{X}_f = [x_f, z_f, \theta_f]^{\mathrm{T}}$ is the displacement vector of the floaters, whose elements represent the surge, heave and pitch displacements respectively. The second term on the left side is the convolution integral that represents the resistive force on the body due to wave radiation, where $\boldsymbol{K}_r$ is the radiation impulse response function; $\boldsymbol{F}_{ext}$ is the wave excitation force vector; $\boldsymbol{F}_B$ is the net restoring force vector due to buoyancy; $\boldsymbol{F}_\nu$ is the viscous damping force vector; $\boldsymbol{F}_{fr}$ is the internal force vector between the rod and the floater; and $\boldsymbol{F}_{ic}$ is the interconnecting force between floater elements.

The inviscid hydrodynamics, i.e., $\boldsymbol{F}_{ext}$, are calculated by using linear coefficients. The convolution term is known as the fluid-memory model, which can be solved by the state-space approximation (Perez and Fossen, 2009). The hydrodynamic coefficients required for the calculation are numerically obtained by the boundary element method (BEM) based on the open-source code, NEMOH (Babarit and Delhommeau, 2015). The viscous damping can be estimated by using a quadratic damping term with empirical drag coefficients, similar to the drag term in Morison's equation (Morison et al., 1950). However, Babarit et al. (2012) pointed out that the estimation of the drag term was negligible when modelling an array of heaving buoys on a fixed platform; hence, we neglect the viscous terms in the present model.

The pistons have only one translational degree of freedom in the heaving direction. Since there will be a control function in the MPP design concept to guarantee that selected pistons can move synchronously, a lumped model is used to describe the motion of the pistons. This means that equivalent piston masses and equivalent cylinder areas are used in the model and will vary according to the piston combinations during the simulation. The motion of a piston is governed by the following equation:

$$m_p \ddot{z}_p = F_{rp} + F_p + F_f, \tag{2}$$

where m_p is the equivalent mass of the piston combination; z_p is the displacement of the piston; F_{rp} is the internal force between the rod and the piston; and F_p is the pumping force, which is a function of the area of the cross section of the cylinder and the dynamics of the piston. F_f is the viscous friction force between the piston and the cylinder, which can be obtained by solving the elastohydrodynamic lubrication (EHL) problem (Vakis and Anagnostopoulos, 2016).

The pumping force F_p can be calculated by Eq. (3) during the upstroke, but becomes zero during the downstroke and is described by

$$F_p = -A_{cc} p_L + \rho \left(L_c + L_U\right) A_{cc} \left(\ddot{z}_p + g\right) + \rho A_{cc} \dot{z}_p^{\,2}, \tag{3}$$

where A_{cc} is the equivalent closing area of the cylinders; p_L is the hydrostatic pressure at the bottom of the lower reservoir; L_c the length of the cylinder; and L_U is the water depth of the upper reservoir.

On the other hand, for the viscous friction force F_f, we consider a simplified formula based on the Couette flow assumption given by

$$F_f = \mu \left(2\pi R_p H_p\right) \frac{\dot{z}_p}{S_p}, \tag{4}$$

where μ is the dynamic viscosity of the fluid; R_p is the radius of the piston; H_p is the height of the piston; and S_p is the piston-cylinder separation. This is a valid approximation when the interface can sustain a lubricant film at all times (except at the bottom and top dead centres) as discussed in the EHL model for a properly selected lubricant.

Since the mass of the rod is much larger than the mass of the piston, the rod is considered as an individual mass body with constant spring and damping coefficients. The upper part (immersed in the sea water) allows three degrees of freedom and the lower part (hidden in the upper reservoir and the cylinders) moves only in the heaving direction. With the additional motion equations of the rod, the internal force (vector) can be obtained.

In the pumping system, due to the significantly large hydraulic head difference between the upper reservoir and the lower reservoir, the pumping force can be very large during the upstroke, which essentially dominates the motion of the piston and strongly influences the motion of the floater via the rod. A discontinuity occurs during switching between the upstroke and the downstroke of the piston. The discontinuous pumping force may reduce numerical stability and introduce non-physical vibrations in the system response. To avert these problems, Vakis and Anagnostopoulos (2016) introduced exponential growth and delay terms to calculate the mass of the fluid column. In this paper, we consider, instead, that the opening and closing of the piston flaps are functions of the relative velocity between the piston and the surrounding fluid, and assume that the variation rate of the closing area of the cylinders is proportional to the velocity of the piston; hereby, the equivalent closing area A_{cc} of the cylinders is expressed as

$$\dot{A}_{cc} = \alpha \dot{z}_p, \tag{5}$$

where α is an empirical coefficient, that can be estimated by experimental data. In this work, we let $\alpha = 18$ during the upstroke and we let $\alpha = 1800$ during the downstroke, the former choice being motivated by experiments where it can be observed that longer times are needed to close the piston flap than to open it. A typical time variation of A_{cc} in the simulation is shown in Fig. 2, where it can be corroborated that the slope of the upstroke

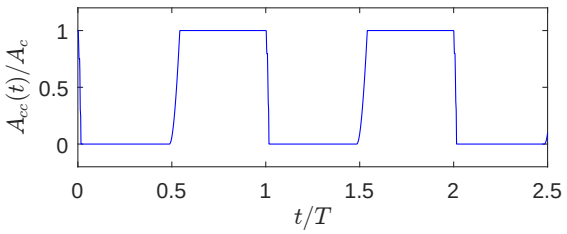

Figure 2: Typical time variation of A_{cc}. A_c is the equivalent area of the cross section of the cylinders, $A_{cc} = A_c$ when the piston flap is fully closed.

is less steep than the slope of the downstroke, since a smaller value of α was used in the upstroke calculation. As will be shown in the following section, non-physical vibrations can be cancelled out by choosing appropriate coefficients.

To solve the system of motion equations in Eq. (1) and Eq. (2) numerically, we rely on WEC-Sim (Wave Energy Converter SIMulator), a MATLAB/SIMULINK based open-source engineering tool (Ruehl et al., 2014). WEC-Sim has the ability to model devices that are

comprised of rigid bodies, such as power-take-off and mooring systems in the time domain. This enables us to rapidly create a numerical model of a floater (blanket) within a block diagram environment. The MPP model is developed using native SIMULINK blocks coupled with WEC-Sim. Fig. 3 shows an example of the model set-up for a single floater with an MPP unit. The "Floater" block represents a floater including the hydrodynamic model, which is originally developed in WEC-Sim. The "Rod" block represents a cable with linear spring and damping forces, whose ends connect to the floater with a revolute joint and to the piston with a planar joint, amounting to the three degrees of freedom for the floater motion as described in Eq. (1). The "Piston" block consists of a piston unit with an equivalent mass; a built-in control module allows us to vary the piston combinations during the simulation, namely the equivalent mass, such that the pumping force and other external forces are calculated based on the dynamics of the piston at the current time step. The "Cylinder" consists of a translational constraint that restricts the piston motion in the heaving direction only. The "Global Reference Frame" acts as the seabed.

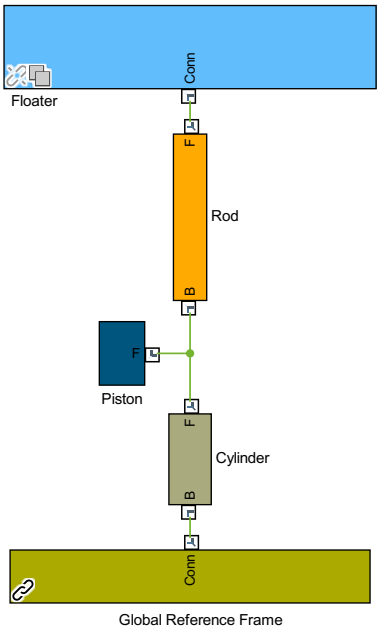

Figure 3: WEC-Sim model setup for a single floater WEC with an MPP unit.

As experimentally observed in van Rooij et al. (2015), the mechanical efficiency of the pumping system is quite high (near 99%), while the volumetric loss of the proof-of-concept pumping system (including the losses of the check valve, piston valve and through the cylinder and piston separation) ranged between 35% and 40%, which essentially dominated the power loss. The leakage due to the piston-cylinder separation will be small in the full scale pumping system, which was investigated in the EHL model (Vakis and Anagnostopoulos, 2016). Further experiments are required to validate these findings and to calculate the total volumetric loss with high accuracy. Since the present work aims to prove the MPP concept rather than quantify the energy output of the full device, it is decided to disregard the volumetric losses in this numerical model. Alternately, instead of the produced power, the pumping power (Eq. (6)) and the pumping energy (Eq. (7)) are used in the discussion in the following. The

pumping power is calculated by the general formula

$$P_p = F_p \dot{z}_p, \tag{6}$$

and integrating the pumping power over a period of time t, yields the pumping energy

$$E_p(t) = \int_0^t P_p(\tau)\, d\tau. \tag{7}$$

The leakage and volumetric losses will be assessed by our ongoing large-scale MPP experiments and accounted for in an upgraded numerical model.

The initial displacements of the floaters are set to their equilibrium positions in still water, which are calculated by taking into account the initial force on the rod. The piston is initially located at L_r (the length of the rod) below the floater. For regular wave simulations, a linear sinusoidal wave with period T and amplitude $H/2$ is used as the incident wave. For irregular wave simulations, the incident wave is a linear superposition of a number of regular wave components. In order to improve the stability of the model, the incident waves are gradually generated with a time ramp function in the simulation.

The capture factor (also known as the capture width ratio) is commonly used to assess the performance of WECs (Renzi and Dias, 2013). It is defined as the ratio between the capture power of the device and the power of the incident wave per unit width of the device, i.e.,

$$C_F = \frac{P_m}{\frac{1}{8}\rho g H^2 c_g D_w}, \tag{8}$$

where P_m is the mean captured power over a wave period, with $P_m(t+T) = \int_t^{t+T} P_p(\tau)\, d\tau/T$ in the present paper; D_w is the width of the floater; and c_g is the group velocity. In this study, we use the capture factor to assess the performance of the Ocean Grazer WEC, as will be discussed in the following section.

3. Results and discussion

In this section, the developed numerical model is compared against the experimental results of the single piston pump (SPP) and the previously developed analytical model from Vakis and Anagnostopoulos (2016). Moreover, a series of simulations with various wave conditions and piston combinations are carried out, in order to understand the MPP performance and demonstrate the adaptability of the MPP concept. Finally, a numerical simulation of the MP^{2}PTO system with ten elements is presented, in order to investigate the hydrodynamic response of the floater blanket and the capture power of the MP^{2}PTO system.

3.1. Model validation

As previously mentioned, the experimental study of the SPP system was carried by van Rooij et al. (2015). The displacement, pumping force and pressure in the reservoirs were

measured in the experiment. The experimental conditions can be numerically reproduced by removing the "Floater" block in Fig. 3, and prescribing the sinusoidal velocity to the end of the rod. All the parameters are the same as those in the experiment, which can be found in van Rooij et al. (2015).

The time histories of the piston displacement, piston velocity, pumping force and pumping power are compared with the experimental results, as depicted in Fig. 4; in this figure, it can be seen that there is very good agreement between the two. The piston velocity is a sinusoid

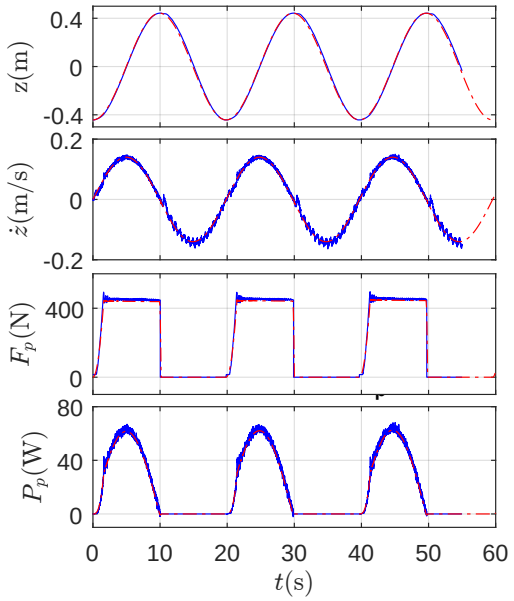

Figure 4: Comparison of numerical results (red dashed lines) and experimental results (blue solid lines) for piston displacement, piston velocity, pumping force and pumping power (top to bottom, respectively). The simulated wave in this case is $H = 0.885$ m, $T = 20.1$ s.

with a saw-tooth-like high frequency modulation in the experiment, but is much smoother in the simulation. Three reasons may cause such a difference: (i) the experimental velocity was obtained by derivating the piston displacement, rather than by measuring it directly; (ii) the stiffness of the frame that supported the pumping system in the experiment might result in additional high-frequency vibrations; (iii) the cable properties, e.g. the spring constant and damping, can influence the vibrational behaviour in the simulation. Because the variable A_{cc} with different coefficients according to Eq. (5) is used during the switching between the up- and down-stroke, the increase and decrease of the pumping force is in good agreement with the measurement. High-frequency oscillations of the pumping force are observed in the experiment after the switching because the sudden change of the pumping force results in slamming. Although similar oscillations are also observed in the simulation, their amplitude is small and not visible in the current plot. The larger amplitude of the oscillation in the experiment might partly be ascribed to the additional vibration of the mounting frame, as previously mentioned. Nevertheless, the accuracy of the present model is satisfactory. The model can be further developed to investigate the MPP unit.

A numerical model of a single box-shape floater (7m $\times$ 7m $\times$ 2m) with an SPP unit was

proposed by Vakis and Anagnostopoulos (2016), hereinafter referred to as the SPP model. The major differences between the SPP model and the present model are summarized as follows: (1) to avoid the numerical issues caused by the discontinuous pumping force, the SPP model used exponential growth and decay terms to calculate the fluid column mass, whereas the present model considers that the closing/opening of the piston flap is a function of the piston velocity; (2) only the heaving motion of the floater is accounted for in the SPP model, while the floater in the present model incorporates three degrees of freedom; (3) the hydrodynamics calculation is simplified in the SPP model, whereas the present model calculates the hydrodynamic forces based on BEM, taking into account the diffraction and radiation effects; (4) a full EHL model is developed to calculate the fluid force in the SPP model, but the present model uses a simplified lubrication model instead.

The comparison of the motion of the floater is presented in Fig. 5, where it can be observed that the displacement and velocity are in good agreement between models. However, significant oscillations are observed in the time series of the acceleration in the SPP model. The oscillations occur at the switching instances between the upstroke and the downstroke, and can be explained as a result of the SPP model neglecting the radiation damping term, while the present model accounts for radiation damping via BEM; hence, this non-physical oscillation does not appear in the present model, which is an improved representation of the system's behaviour (as can be observed in the comparison with experiments in Fig. 4).

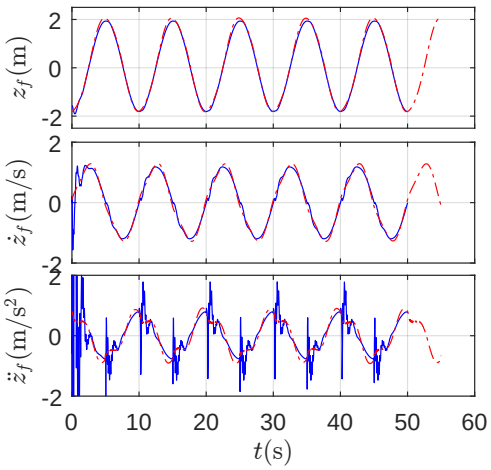

Figure 5: Comparison of the floater motion between the present numerical model (red dashed lines) and the SPP model (blue solid lines). The incident wave in this case is $H = 4.0$ m, $T = 10$ s.

The time-history comparison of the piston dynamics, pumping force and pumping power between the two models is presented in Fig. 6. The agreement of the piston dynamics between the two models is not as good as that of the floater dynamics shown in Fig. 5. The amplitude of the displacement is consistent between models, but the time variation has a slight difference. This difference may be caused by the different treatment of the rod motion. In the SPP model, the piston and the rod are considered as one ensemble, namely a lumped mass model, while, conversely, in the present numerical model, they are calculated separately and the part of the rod immersed in the sea water is allowed to have three degrees

of freedom. Consequently, since the piston velocity in the present model is slightly larger, the capture power is also higher. Lastly, the pumping force between the SPP model and the present model matches almost perfectly, except for the large spike at the switching that should be caused by the sudden change in fluid column mass in the SPP model. Note that the oscillation during the upstroke is observed in both models, due to the spring effect of the rod.

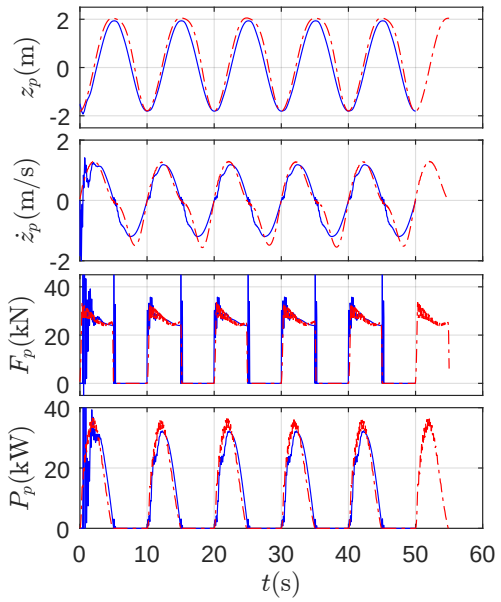

Figure 6: Results comparison between the present numerical model (red dashed lines) and the SPP model (blue solid lines) corresponding to piston displacement, piston velocity, pumping force and pumping power (top to bottom, respectively).

Following the latter comparison between the SPP model and the present numerical model discussed in this section, we provide the following summary. Firstly, the SPP model used a purely numerical treatment to deal with the discontinuous pumping force, while the time variation of A_c is used to physically describe the opening/closing of the piston flap in the present model; the aforementioned time variation can be obtained experimentally. Therefore, the accuracy of the present model can be further improved by performing a set of experiments to determine the empirical coefficients in Eq. (5). Secondly, the inclusion of additional degrees of freedom in the floater, as done in the present model, does not significantly influence the heaving motion of the single floater. However, in the hydrodynamic model of the floater blanket, the floater elements are interconnected, and their pitch motion has to be accounted for. The multi-degree of freedom motion is essential for the floater blanket model. Furthermore, according to the present results, it is found that the excitation force and the net restoring force dominate the floater dynamics. Hence, the simplification of the hydrodynamics in the SPP model is acceptable for the single floater model. However, as will be shown in the following section, the diffraction and radiation effects may significantly influence the dynamics of the floater elements and the energy extraction for short-period waves. These should be carefully calculated, and, thus, the SPP model is not applicable in this case. Finally, the effect of the fluid friction in the dynamics of the pumping system is found to be

insignificant; hence, the simplified calculation is sufficient for the present numerical model, especially because using a full EHL model requires very small time steps to deal with the high frequency vibration of the piston, which is computationally inefficient. Accordingly, a full EHL model is not applied in the present numerical model. In conclusion, the present model is a more comprehensive model regarding the hydrodynamics and multibody system dynamics with respect to the SPP model. Thus, it can be applied in the investigation of the floater blanket and the MP^{2}PTO system.

3.2. Single floater with MPP unit

The core innovation of the Ocean Grazer is that an MPP unit can realize multiple piston combinations, which can adapt to incoming wave heights and periods in order to maximize energy extraction. In this section, the numerical model of a single floater with an MPP unit is used to illustrated this adaptability and demonstrate the validity of the MPP concept.

According to our numerical testing, we initially design an MPP unit of three pistons with different masses and radii, whose parameters are outlined in Table 1. Based on the current

Table 1: Parameters of the MPP unit used in the simulation.

Piston No.	mass (kg)	radius (m)
1	200	0.2
2	400	0.3
3	700	0.4

MPP design, we can obtain seven different piston combinations with various equivalent piston masses and areas, as presented in Table 2. Corresponding to the selected set, the equivalent mass of the piston in the model is altered according to Table 2, and the pumping force is calculated by using the equivalent area during the simulation, which will result in a different dynamic response of the multibody system. By selecting the optimal piston combinations to deal with the varying incident waves, the MPP unit is expected to extract more energy

Table 2: Seven piston combinations in an MPP unit (0 = inactive and 1 = active in the piston combination); furthermore, m_p is the equivalent mass of the pistons and A_c is the equivalent area of the cylinders.

Set No.	combination	m_p(kg)	A_c(m^2)
1	{1, 0, 0}	200	0.126
2	{0, 1, 0}	400	0.283
3	{1, 1, 0}	600	0.408
4	{0, 0, 1}	700	0.502
5	{1, 0, 1}	900	0.628
6	{0, 1, 1}	1100	0.785
7	{1, 1, 1}	1300	0.911

than those using the constant piston combinations. It should be noted that the effect of the coupling mechanism to the dynamics of the system is assumed to be negligible; this is necessary, pending the finalization of the mechanism's design.

To demonstrate the potential of an MPP unit, a set of simulations with the seven different possibilities stated in Table 2 is carried out with a wide range of wave periods and wave heights. The mean power over one wave period and the capture factor of the WEC are calculated in each simulation. Accordingly, these results are expressed in matrix form, showing the power factor capture C_F as a function of the wave period T and wave height H, which can indicate the energy extraction efficiencies across sea states. The capture factor matrices corresponding to the seven sets are shown in Fig. 7. In this figure, it can be seen that the energy extraction is definitely influenced by the selection of the piston combinations. For example, the capture factor of *set7* is about 6 times that of *set1* for the wave of $T = 8$ s and $H = 5$ m; in contrast, *set7* captures only 1/6 of the energy captured by *set1* for the wave of $T = 8$ s and $H = 1$ m, which implies that selecting an appropriate piston combination during operation can significantly improve the device performance. These seven matrices also indicate that each set has its own zone with relatively high capture factors. Ideally, for each specific incident wave, one can choose the optimum set of the seven to enlarge the high capture factor zone, as shown in the last plot of Fig.7. The MPP can achieve roughly the same high capture factor for the waves with various wave heights and the same wave periods. The highest performance is obtained at $T = 6$ s, but the capture factors decrease as the wave periods increase; this behavior is related to the device specifications. Optimizing these specifications, i.e., the sizes and masses of the floater and the pistons, may enable the device to work well for even longer period waves; this will be investigated in the future.

To take advantage of the adaptability of the MPP unit, we identify the set which captures maximum power (or has the highest capture factor) as the optimum set, based on the numerical results presented in Fig. 7. The matrix representation of the optimum set under various wave conditions is shown in Fig. 8, which corresponds to the combinations presented in Table 2. These results suggest that a lighter combination should be chosen for both short-period waves and long-period waves while the heavier combination is favorable for intermediate-period waves; furthermore, heavy combinations are always recommended for waves with large amplitudes.

The indexing matrix discussed thus far is obtained based on a monochromatic wave simulation, but such a sea state is rare in reality and can only be found in wave tank tests. In order to apply the results of the indexing matrix to a more realistic wave sea state, we consider incident waves presented as continuous time series with variable wave heights and periods. A simple algorithm is used to determine the current wave heights and periods, as explained and sketched in Fig. 9. Note that this procedure to determine the wave heights and periods does not have a real physical meaning, but aims to make use of the indexing matrix to control an MPP unit. Once the time varying wave heights and periods are obtained, a lookup table is used to index the optimum set during the simulation. Accordingly, the piston combination switches to its optimal combination as soon as the piston velocity transitions from negative to positive (during the upstroke). Therefore, the MPP unit can adapt itself to the varying incident waves. This approach is an initial attempt aiming to test the MPP concept, even though it is simple and only considers the wave dynamics for the combination selection. In

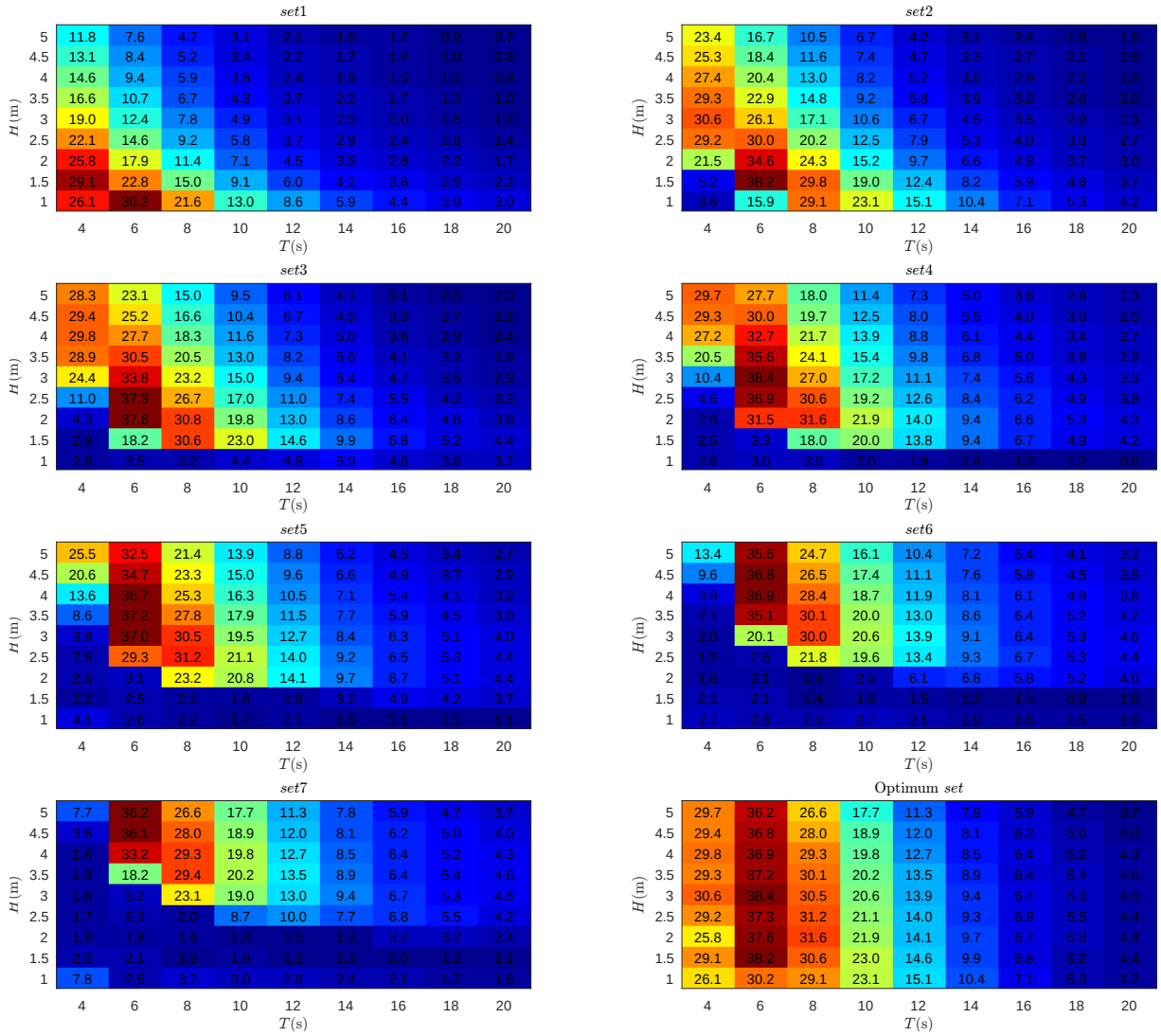

Figure 7: Capture factor matrix of a WEC with a single floater and an MPP unit. The values in the plots are the capture factor (scaled by a factor 10^{-2}) using constant piston combinations. The last plot shows the ideal capture factor by using optimum piston combinations.

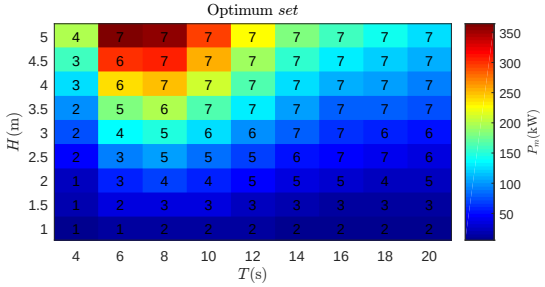

Figure 8: Optimum set indexing matrix of a WEC with a single floater and an MPP unit. The color represents the maximum mean power in the seven sets under the same wave condition, the number indexes the optimum set which can capture the maximum energy under the specific wave condition.

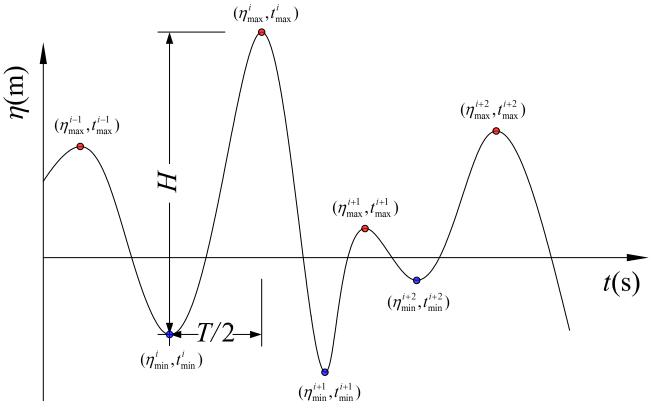

Figure 9: Procedure to obtain wave heights and periods in an incident wave series with varying height and period. A loop is used to find the local maxima (η_{max}) and minima (η_{min}) in the time series of wave elevation. The wave height is calculated by $H(t) = \eta^i_{max} - \eta^i_{min}$ and the wave period is determined by $T(t) = 2\left(t^i_{max} - t^i_{min}\right)$, where $i \in \{0, 1, .., n.\}$.

broad terms, the piston dynamics in the MPP unit are not only determined by the incident wave at the current time, but are also influenced by the fluid-memory effects associated with the radiation forces exerted on the floater, and the mechanics of the interconnection between the parts of the device. Hence, the development of a suitable control algorithm for an MPP unit should take into account the dynamics of the floater and the piston; this is left for future work.

Subsequently, the simulation of a single floater with an MPP unit under irregular waves is carried out to validate the adaptability of the MPP concept. Furthermore, simulations with the other seven constant piston combinations are added to the comparison. Special attention should be paid when comparing the simulation results under irregular incident waves. When applying a wave spectrum to generate a wave series, the wave is essentially created by the superposition of a finite number of waves having different phase, frequency and amplitude. The wave field may be different depending on the sets of chosen phases. In the present paper, the same random phases are used for all cases, in order to be consistent with the incident waves in the simulations. The time histories of energy extraction are shown in Fig. 10. In this figure, it can be observed that *set1* can extract energy stably because its light pumping load allows it to pump the fluid with very low waves, but the disadvantage is that its capture power is small. The total extracted energy is only half of that captured by the MPP unit in the present study. The pumping load of *set7* is the heaviest, and wave forces are not strong enough to lift the pistons for most of the time during the simulation. Thus, *set7* only captures little energy from the beginning to $t = 270$ s, which would seem to suggest that a redesign of the MPP configuration is necessary. However, on the occasion of large incident waves, the capture power is significantly large, e.g., as in the step-like increase of energy extraction that can be observed at $t = 270$ s. The intermediate combinations e.g., *set2* and *set3*, show better performance than other constant combinations under the current moderate sea state. Note that the result corresponding to the MPP unit in Fig. 10 clearly

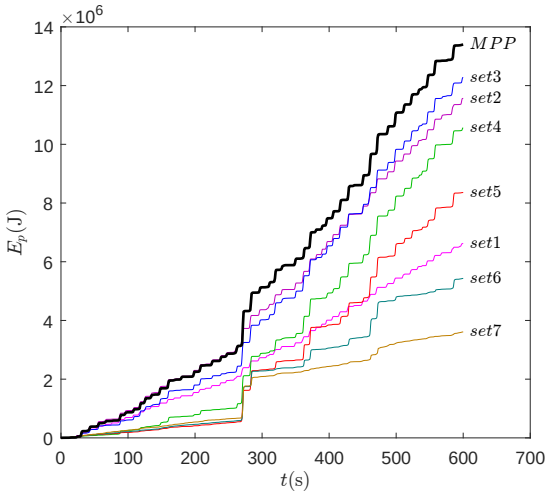

Figure 10: Comparison of extracted energy with various constant piston combinations and an adaptable MPP unit. The time series of the incident wave in the present study is generated by JONSWAP spectrum with $H_{m0} = 2.0$ m and $T_p = 12$ s.

outperforms the seven constant piston combinations, thanks to the adaptability of the MPP unit.

Fig. 11 shows the time histories of irregular wave elevation and the corresponding set used during the simulation. At the beginning of the simulation when the incident wave is weak,

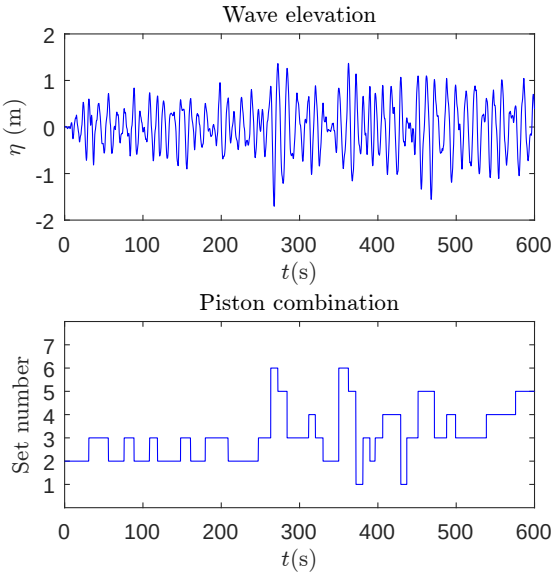

Figure 11: Selection of optimum set during irregular wave series (Top: time series of wave elevation. Bottom: corresponding piston combination).

light combinations are adopted, such that the combinations switch between *set2* and *set3*. When encountering a strong wave event, e.g., at $t = 270$ s, the combination switches to *set6*, a relatively heavier selection. As soon as the strong wave event has passed, the lighter combination is adopted once again. As can be corroborated in Fig. 10, the final results are

Table 3: Mean capture power under various wave conditions with different piston combinations.

	$H_{m0} = 1.0$ m, $T_p = 12$ s			$H_{m0} = 2.0$ m, $T_p = 12$ s			$H_{m0} = 3.0$ m, $T_p = 12$ s		
	P_p(kW)	%	#	P_p(kW)	%	#	P_p(kW)	%	#
set1	4.39	96.30%	2	11.03	49.40%	6	17.75	36.20%	8
set2	4.09	89.70%	3	19.27	86.30%	3	34.34	70.10%	6
set3	2.48	54.40%	5	20.46	91.60%	2	43.10	87.90%	4
set4	1.67	36.50%	7	17.60	78.80%	4	46.31	94.50%	2
set5	1.54	33.70%	8	13.93	62.40%	5	44.87	91.50%	3
set6	1.97	43.30%	6	9.06	40.60%	7	36.82	75.10%	5
set7	2.53	55.40%	4	6.02	26.90%	8	31.02	63.30%	7
MPP	4.56	100.00%	1	22.33	100.00%	1	49.02	100.00%	1

that the adapting MPP unit can extract about 10% more energy than the optimum constant combination, i.e., *set3*.

More simulations are carried out to further validate the MPP concept under various sea states. The mean capture power with various wave conditions is shown in Table 3. The results indicate that the MPP unit can always capture the maximum energy from the ocean wave compared to the other seven constant piston combinations, and the mean power is 3.7% to 8.5% greater than that of the optimum constant combinations. Based on the numerical results, it is concluded that it is crucial to select the appropriate piston combinations under the specific sea state; inappropriate combinations may significantly reduce the capture power by over 70%, and developing a control strategy for an MPP unit will indeed be valuable for the Ocean Grazer WEC.

Although the present study demonstrates that the MPP concept can take advantage of its adaptability to maximize energy extraction in various wave conditions, we acknowledge that the design of the floater element and the MPP unit should be further optimized, in order to obtain a high capture factor over wide ranges of wave heights and periods. In addition, the control strategy of the MPP unit is very simple in the present study: it does not access the information from the floater and piston dynamics. Moreover, the wave elevation used in the control is known in advance rather than based on a real-time prediction. Development of an MPC strategy for the MPP unit, based on the present numerical model, is a work in progress. It is expected that a superior control strategy can significantly improve the MPP performance.

3.3. Floater blanket with MP^{2}PTO system

A single floater with an MPP unit can only extract a limited amount of energy. A grid of interconnected floater elements (floater blanket) is designed for the MP^{2}PTO system, aiming to sequentially extract energy from ocean waves as they move through the WEC. Because the length of the floater blanket may be comparable with the wavelength, the diffraction and radiation cannot be neglected in this case. As opposed to the single floater device, where

the radiation is dependent only on the single floater's own motion, additional interaction forces arise between the floater elements from two aspects: (1) the floater elements are physically interconnected with each other, and their motion must be coordinated with that of their neighbours; (2) the presence of the floaters (diffraction effects) and the motion of nearby floaters (radiation effects) will alter the local wave field that will further influence their motion. The multi-body system dynamics can be solved in the Simscape Multibody$^{\text{TM}}$ environment, and wave and multi-body interaction can be dealt with using NEMOH. A numerical model of a floater blanket consisting of ten floaters has been developed, as shown in Fig. 12. In the original design, the floater blanket may be secured to the Ocean Grazer, a massive platform of hundreds of meters in diameter. In the present model, the platform is not accounted for, but a constraint is introduced to the first element of the floater blanket to restrict its surge motion.

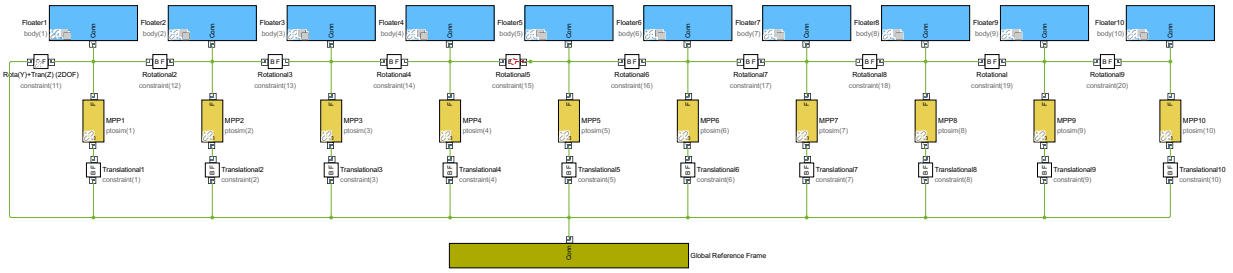

Figure 12: WEC-Sim model set-up for the floater blanket. Each floater is connected to an individual MPP unit. The floater elements are interconnected by revolute joints, which only allow relative rotation between their neighbours. Furthermore, a pin slot joint is applied on the first floater at the left to restrict its surge motion.

Simulations for four cases with various wave periods are carried out to understand the hydrodynamic response of the floater blanket and the MP^{2}PTO performance. Due to the lack of knowledge about the optimum MP^{2}PTO configuration at the present stage, a constant piston combination (*set1*) is used for all MPPs in the simulation. The resulting mean power for each MPP is presented in Fig. 13. The extracted power of the MPPs decreases along the

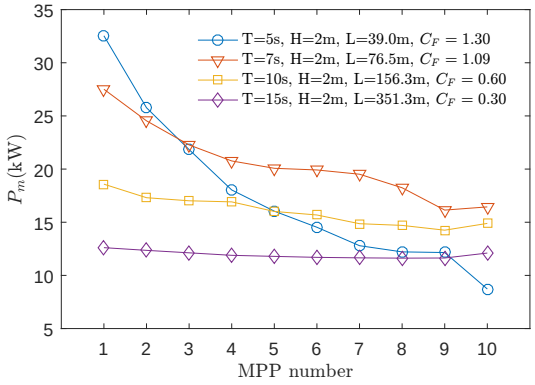

Figure 13: Mean capture power of each MPP under various wave conditions.

wave direction for short-period waves in general, i.e., the cases of $T = 5$ s and $T = 7$ s. Note

that MPP1 captures five times more energy than MPP10 in the wave of $T = 5$ s. However, the mean power of the MPPs is almost constant for long-period waves, i.e., $T = 15$ s. This is because the diffraction effects are generally more pronounced for waves whose wavelength is roughly comparable to the dimensions of the obstacle. The wavelength of a $T = 5$ s period wave is 39 m, which is about half the length of the floater blanket (70 m); thus, the incident wave is partly diffracted away from the floater blanket, resulting in a decrease in captured power along the wave direction. The wavelength of a $T = 15$ s period wave is five times greater than the length of the floater blanket; thus, the long wave can easily transit through the floater blanket without any significant disturbance on the wave profile, so that each MPP unit exhibits similar performance. The capture factor of each simulation is also stated in Fig. 13. The capture factor can be greater than one for the short-period waves, because elongated floating bodies should diffract waves, which will be concentrated in the downwave direction, as stated by Rainey (2001), and can maintain the energy input for the following floaters. Although the incident waves are diffracted at the front of the floater blanket resulting in energy loss, there will be energy compensation from the sides. The capture factor decreases dramatically as the period of the waves increases, due to the fact that the stiffness of a heaving buoy should be very high in order to oscillate in resonance with the system (Payne et al., 2015).

The hydrodynamic response of the floater blanket under various incident waves can be understood by comparing the excitation force on the floater elements, as presented in Fig. 14. The excitation force on the individual floaters decreases sharply from the first floater to

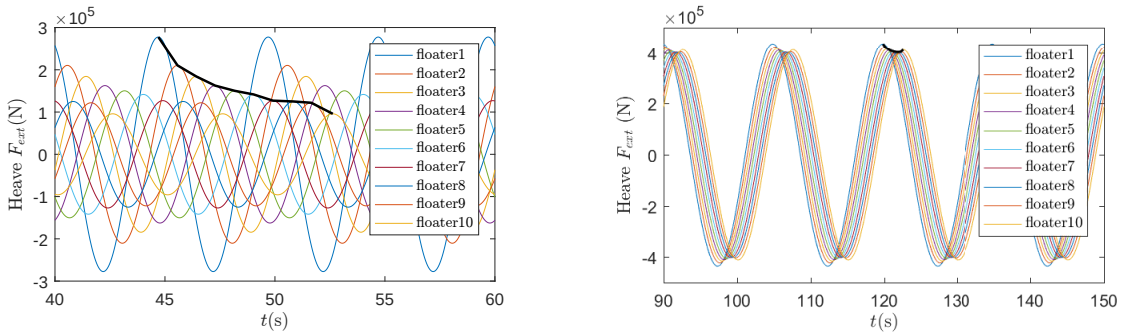

(a) $T = 5$ s, $H = 2$ m (b) $T = 15$ s, $H = 2$ m

Figure 14: Time histories of the excitation force on the floater elements. The evolution in amplitude of the excitation is marked with a bold black line, to exemplify the decay in (a) and the slight increase towards the end of the floater blanket in (b).

the tenth in the short-period wave cases, as can be seen clearly from the black bold line in Fig. 14a, which represents the trend of the amplitude of the force. This explains why the capture power decreases in the wave direction. However, there is only a slight difference between the floater elements in the longer-period waves. Interestingly, the amplitude of the excitation force does not decrease monotonically for long-period waves. It decreases at the first few floaters, but increases at the end; therefore, the energy extraction for each MPP is roughly the same and MPP10 can capture slightly greater power.

In order to shed some light on the influence of the PTO configuration on the hydrodynamic

response of the floater blanket and the energy extraction, we perform further simulations in the sequel using the ten floater model. The results are presented in Fig. 15 for the sets with seven constant piston combinations under two waves with same wave amplitudes but different periods. In the short-period wave case (Fig. 15(a)), the capture factor is greatest

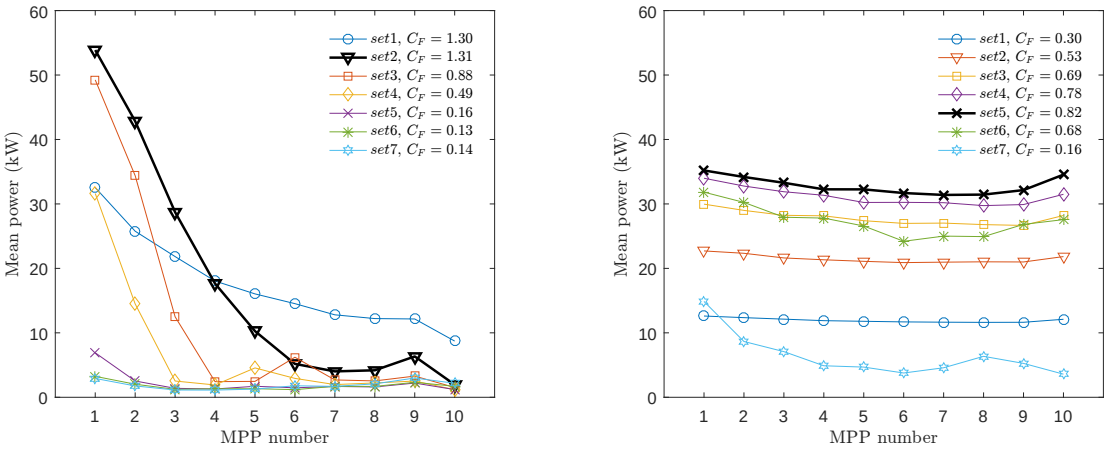

(a) $T = 5$ s, $H = 2$ m (b) $T = 15$ s, $H = 2$ m

Figure 15: Time histories of excitation force on each floater for (a) a short-period wave; and (b) a long-period wave.

for the lightest combination (*set1*). *Set2* captures slightly less energy than *set1*, but the difference in mean power between the ten MPPs is much larger; the mean power of MPP1 is about 57 kW, whereas for MPP10, this is only 3 kW. The previous can be physically explained, since choosing *set2* for MPP1 results in the extraction of more energy than with *set1*; hence, less energy is delivered to the later MPPs. Although the mean power of MPPs 1-3 of *set2* is higher than that of *set1*, MPPs 6-10 hardly capture any energy. As a result, the overall energy extraction of *set2* is less than that of *set1*. For the relatively heavier combinations, i.e., *sets 5-7*, the floater blanket keeps almost stationary; hence, the MPPs only extract little energy. The capture factors decrease as the piston combinations become heavier, indicating that the lighter piston combination is a better choice under the current wave condition. It is interesting to see that the mean power of each MPP does not decrease monotonically. Spikes can be observed in some sets, e.g., MPP9 under *set2*, MPP6 with *set3* and MPP5 using *set4*. Such phenomena also appear occasionally in our initial experimental testing. This could be caused by the superposition of the diffracted and radiated waves with the incident waves, resulting in increased floater heaving at specific positions. This issue should be investigated by developing an analytical model in the future. The present results imply that the incident wave field has been altered due to the diffracted and radiated waves by other floaters. Hence, the lookup table based on the indexing matrix from the single floater simulation in Fig. 8 is not applicable for controlling the individual MPP in MP^{2}PTO system under the short-period waves.

For the long-period wave case (Fig. 15(b)), the capture factors increase from *set1* to *set5*, but decrease afterwards. The ten MPPs can gain similar energy except with *set7*, in which a spike is observed at MPP8. It seems that a constant piston combination (*set5*) is the

optimum set for the MP^{2}PTO because all 10 MPPs can always capture the maximum power with *set5*. When indexing the wave condition of $T = 15$ s and $H = 2$ m in Fig. 8, we find that the optimum set for the single floater is *set5*, which is the same as the current case of the floater blanket. Thus, we can conclude that the lookup table in Fig. 8 is likely valid for the floater blanket under the long-period waves.

The MP^{2}PTO concept allows each MPP to select a different piston combination independently, to deal with the altered ocean waves. As previously discussed, the wave profile at the site of the floater elements is significantly different in the short-period waves; hence, selecting the optimum set for each MPP may increase the overall energy extraction. Since *set0* $= \{0, 0, 0\}$, where no pistons are activated within an MPP is the eighth combination in addition to the aforementioned seven configurations, an MP^{2}PTO system with ten MPP units will have 8^{10} possible configurations and it is computationally expensive to perform a combinatorial search for finding the optimum configuration. Other heuristic approaches, such as genetic algorithms or branch-and-bound algorithms, can be considered to obtain the sub-optimum solution with less computational demands than the exhaustive enumeration approach. In the present work, we attempt to use the guess-and-check approach to search for the optimum configuration for the MP^{2}PTO in short-period waves.

As shown in Fig. 14(a), the extraction force decreases along the wave direction, suggesting that the sets of MPPs with the same tendency may result in better performance. We design the simulation of eleven configurations, i.e., *conf.1* to *conf.11*, as presented in Table 4. The

Table 4: Configurations of the MP^{2}PTO system used in the simulation, the numbers in the table correspond to the MPP set described in Table2.

MPP No.	1	2	3	4	5	6	7	8	9	10
conf.1	1	1	1	1	1	1	1	1	1	1
conf.2	2	2	1	1	1	1	1	1	1	1
conf.3	3	3	2	2	1	1	1	1	1	1
conf.4	4	4	3	3	2	2	1	1	1	1
conf.5	5	5	4	4	3	3	2	2	1	1
conf.6	6	6	5	5	4	4	3	3	2	2
conf.7	7	7	6	6	5	5	4	4	3	3
conf.8	7	7	7	7	6	6	5	5	4	4
conf.9	7	7	7	7	7	7	6	6	5	5
conf.10	7	7	7	7	7	7	7	7	6	6
conf.11	7	7	7	7	7	7	7	7	7	7
conf.12	7	6	6	6	5	5	5	5	4	4

configuration of the MPPs starts from the uniform *set1*, increases gradually in size/load along the wave direction, and ends at the uniform *set7*. Each MPP gets a chance to vary the *set* from 1 to 7. The mean power of the MPPs and the overall capture factor by using these MPP configurations are shown in Fig. 16. As we use a relatively large amplitude wave in the study, the configuration *conf.1* consisting of uniform *set1* extracts the least amount of energy. The captured power increases by using *conf.2*, in which MPP1 and MPP2 are

changed to *set2*. The capture factors increase as the loads of the MPPs increase until *conf.7*, and decrease afterwards. The results suggest that *set7* should be applied to MPP1, but the lighter set may be better for the following MPPs because the wave excitation decreases. Based on the results from cases *conf.1* to *conf.11*, we pinpoint the sets which obtain the maximum mean power as the optimum sets for each MPP. These sets are finally selected as *conf.12*. The result attained by *conf.12* is encouraging. The device with this configuration obtains the highest capture factor of 2.46 among all 12 configurations. We acknowledge that configuration *conf.12* may be not the optimal configuration out of all possibilities, but it demonstrates the advantage of the adaptability of the MP^{2}PTO system: one can vary the sets of MPPs to maximize the energy extraction. This is a complex optimal control problem, which should account for waves and multi-body interactions, as well as the multi-body system dynamics, and will be a great challenge in our further work.

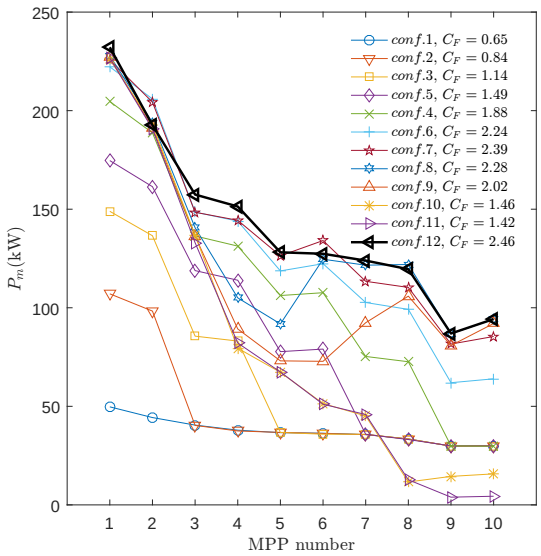

Figure 16: Mean power of MPPs in various MP^{2}PTO configurations (using $T = 7$ s, $H = 3.5$ m).

It is emphasized that the present work only focuses on the validation of the MP^{2}PTO concept working principle, rather than on predicting the energy output of the Ocean Grazer WEC. The capture factor presented here only indicates its dependency on the wave conditions and the MP^{2}PTO configurations, but the overall performance of the full scale device will be definitely improved by applying an optimized design of the floater blanket and developing a high-efficiency control system for the MP^{2}PTO system. Additionally, the efficiencies of the turbine system (shown as T in Fig. 1) and the delivery to the power grid should be considered.

The present models deal with the floater blanket in the open sea, but, in the original Ocean Grazer design, the floater blanket should be mounted in the channels of the platform. The hydrodynamic response of the floater blanket in the channel may exhibit a different behaviour. Our initial experiment has demonstrated that there was a phase shift between the motion of floaters and the motion of waves, while there is no significant phase difference in the current open-sea simulation. The channel version of the numerical model is a work in

progress, in order to compare it with experimental results in a wave tank.

4. Conclusions and further work

The present work has used a time domain numerical model to investigate the hydrodynamics of the floater blanket and demonstrate the adaptability of the MP^{2}PTO system. The proposed model takes into account the diffraction and radiation effects via NEMOH, and allows the inclusion of multiple degrees of freedom for the floater elements. The model is validated by comparing the dynamics of the floater and pistons with our experimental results and a previously developed model, achieving good agreement with both.

Numerical results of a single floater with an MPP unit indicate that the MPP concept can potentially improve the device performance in a wide range of wave periods and heights. The irregular wave simulations demonstrate that the adapting MPP unit, by means of a simple control algorithm, can extract more energy than other constant piston combinations.

Moreover, a numerical model consisting of ten interconnected floater elements within the MP^{2}PTO system is proposed and investigated. The floater elements present similar hydrodynamic responses to long-period waves, but their motion may be seriously affected by diffraction and radiation effects under short-period waves. Therefore, the simple control algorithm based on the results of the single floater is not applicable for controlling the MP^{2}PTO system under short-period waves, but is likely valid under long-period waves. In addition, the overall energy extraction by the MP^{2}PTO system can be improved by optimizing the set of MPPs.

Experiments of a scale prototype of the floater blanket are planned, which will focus, not only on the energy extraction, but also on the wave propagation and the dynamics of the floater elements. The main purpose of the experiments is to understand the hydrodynamics of the floater blanket and search for the optimal configurations of the MP^{2}PTO system under various wave conditions. It also offers a benchmark for validating the numerical model. Another large-scale MPP prototype experiment is a work in progress, and aims to investigate the hydraulic characteristics and efficiency of an MPP unit. With the two experiments and via additional assumptions, we expect to estimate the overall efficiency of the device and its total energy output.

The proposed time domain model is time consuming, with its computational cost depending on the degrees of freedom added to the model. A typical model consisting of ten floater elements takes approximately one day to run, corresponding to 200 seconds of physical time. This makes it difficult to identify the optimal configurations of the MP^{2}PTO system via a large number of guess-and-check simulations. A frequency domain analytical model may be an alternative, and in that context, it may offer a guideline for developing a control strategy for the MP^{2}PTO system. Therefore, development of an analytical model in the frequency domain will be of great value. This is the focus of future work, as is the development of MPC strategies for the single and ten-element piston pump model.

References

Alam, M.-R., 2012. Nonlinear analysis of an actuated seafloor-mounted carpet for a high-performance wave energy extraction. Proceedings of the Royal Society of London A: Mathematical, Physical and Engineering Sciences.
URL http://rspa.royalsocietypublishing.org/content/early/2012/06/11/rspa.2012.0193

Babarit, A., Delhommeau, G., 2015. Theoretical and numerical aspects of the open source BEM solver NEMOH. In: 11^{th} European Wave and Tidal Energy Conference (EWTEC2015).

Babarit, A., Hals, J., Muliawan, M., Kurniawan, A., Moan, T., Krokstad, J., 2012. Numerical benchmarking study of a selection of wave energy converters. Renewable Energy 41, 44 – 63.

Barradas-Berglind, J., Meijer, H., van Rooij, M., Clemente Pinol, S., Galvan Garcia, B., Prins, W., Vakis, A., Jayawardhana, B., 2016. Energy capture optimization for an adaptive wave energy converter. In: Proceedings of 2^{nd} International Conference on Renewable Energies Offshore. CRC Press, Taylor and Francis Group, pp. 171–178.

Dijkstra, H., Barradas-Berglind, J., Meijer, H., van Rooij, M., Prins, W. A., Vakis, A., Jayawardhana, B., 2016. Revenue optimization for the Ocean Grazer wave energy converter through storage utilization. In: Proceedings of 2^{nd} International Conference on Renewable Energies Offshore. CRC Press, Taylor and Francis Group, pp. 207–213.

Haren, P., Mei, C. C., 1982. An array of Hagen-Cockerell wave power absorbers in head seas. Applied Ocean Research 4 (1), 51 – 56.
URL http://www.sciencedirect.com/science/article/pii/S0141118782800217

Li, Y., Yu, Y.-H., 2012. A synthesis of numerical methods for modeling wave energy converter-point absorbers. Renewable and Sustainable Energy Reviews 16 (6), 4352 – 4364.
URL http://www.sciencedirect.com/science/article/pii/S1364032111005351

McCormick, M., 1981. Ocean wave energy conversion. Alternate energy. Wiley.

Morison, J., Johnson, J., Schaaf, S., et al., 1950. The force exerted by surface waves on piles. Journal of Petroleum Technology 2 (05), 149–154.

Payne, G. S., Pascal, R., Vaillant, G., 2015. On the concept of sloped motion for free-floating wave energy converters. Proceedings of the Royal Society of London A: Mathematical, Physical and Engineering Sciences 471 (2182).
URL http://rspa.royalsocietypublishing.org/content/471/2182/20150238

Perez, T., Fossen, T. I., 2009. A matlab toolbox for parametric identification of radiation-force models of ships and offshore structures. Modeling, Identification and Control 30 (1), 1–15.

Prins, W., 10 2013. Method and system for extracting kinetic energy from surface waves of a water.

Rainey, R., 2001. The Pelamis wave energy converter: it may be jolly good in practice, but will it work in theory. In: Proceedings 16^{th} International Workshop on Water Waves and Floating Bodies. Hiroshima, Japan.

Renzi, E., Dias, F., 2013. Hydrodynamics of the oscillating wave surge converter in the open ocean. European Journal of Mechanics-B/Fluids 41, 1–10.

Ringwood, J. V., Bacelli, G., Fusco, F., 2014. Energy-maximizing control of wave-energy converters: the development of control system technology to optimize their operation. IEEE Control Systems 34 (5), 30–55.

Ruehl, K., Michelen, C., Kanner, S., Lawson, M., Yu, Y.-H., June 2014. Preliminary verification and validation of WEC-Sim, an open-source wave energy converter design tool. In: Proceedings of the 33^{rd} International Conference on Ocean, Offshore and Arctic Engineering. American Society of Mechanical Engineers, San Francisco, USA.

Vakis, A., Anagnostopoulos, J. S., 2016. Mechanical design and modeling of a single-piston pump for the novel power take-off system of a wave energy converter. Renewable Energy 96, Part A, 531 – 547.
URL http://www.sciencedirect.com/science/article/pii/S0960148116303780

van Rooij, M., Meijer, H., Prins, W. A., Vakis, A., May 2015. Experimental performance evaluation and validation of dynamical contact models of the Ocean Grazer. In: OCEANS 2015 - Genova. pp. 1–6.